Crystallographic, Spectroscopic, and Computational Analysis of a Flavin C4a−Oxygen Adduct in Choline Oxidase[†,‡]

Allen M. Orville,[*,§] George T. Lountos,[||,⊥] Steffan Finnegan,[#] Giovanni Gadda,[*,#,+] and Rajeev Prabhakar[*,▽]

Biology Department, Brookhaven National Laboratory, Upton, New York 11973-5000, School of Chemistry and Biochemistry, Georgia Institute of Technology, Atlanta, Georgia 30332-0400, Department of Chemistry, Georgia State University, Atlanta, Georgia 30302-4098, Department of Biology, Georgia State University, Atlanta, Georgia 30302-4010, The Center for Biotechnology and Drug Design, Georgia State University, Atlanta, Georgia 30302-4098, and Department of Chemistry, University of Miami, Coral Gables, Florida 33146-0431

Received October 13, 2008; Revised Manuscript Received December 2, 2008

ABSTRACT: Flavin C4a−OO(H) and C4a−OH adducts are critical intermediates proposed in many flavoenzyme reaction mechanisms, but they are rarely detected even by rapid transient kinetics methods. We observe a trapped flavin C4a−OH or C4a−OO(H) adduct by single-crystal spectroscopic methods and in the 1.86 Å resolution X-ray crystal structure of choline oxidase. The microspectrophotometry results show that the adduct forms rapidly in situ at 100 K upon exposure to X-rays. Density functional theory calculations establish the electronic structures for the flavin C4a−OH and C4a−OO(H) adducts and estimate the stabilization energy of several active site hydrogen bonds deduced from the crystal structure. We propose that the enzyme-bound FAD is reduced in the X-ray beam. The aerobic crystals then form either a C4a−OH or C4a−OO(H) adduct, but an insufficient proton inventory prevents their decay at cryogenic temperatures.

Although flavins and flavoproteins were discovered in the 1930s, their remarkable functional diversity continues to be characterized. It is now estimated that up to 4% of microbial or eukarytotic proteins are flavoproteins, and more than 1200 flavoprotein structures are currently available from the Protein Data Bank. Flavin-dependent proteins catalyze a wide range of biochemical reactions, including aerobic and anaerobic metabolism, light emission, photosynthesis, DNA repair, plant phototropism, regulation of biological clocks, and the activation of oxygen for hydroxylation and oxidation reactions (*1*). This diversity derives from the flavin isoalloxazine ring system, which is ideally suited for oxidative or reductive reactions involving one- or two-electron transfer to and from other redox-active centers, as well as reactivity with molecular oxygen. Moreover, the isoalloxazine ring system can act as an electrophile or a nucleophile forming covalent adducts with either protein residues or reaction intermediates at the C4a, N5, C6, and C8M positions (see Figure 2 for nomenclature). The flavin is also influenced by the protein active site, which extends the reaction diversity and facilitates catalysis along a particular flavoenzyme reaction coordinate. Thus, the interactions among the flavin, active site residues, and substrate molecules yield almost limitless combinations and, consequently, remarkable diversity in flavoprotein function.

The reaction of molecular oxygen with reduced flavoenzymes is fundamental to all aerobic organisms and can be orders of magnitude faster or slower than the analogous reactions of flavins in solution (*2*). The outcome of the reaction also varies greatly and has been used to segregate flavoenzymes into different classes. For example, the NAD(P)H-dependent monooxygenases cleave the dioxygen O−O bond with incorporation of one oxygen atom into an organic product, and the other oxygen atom is then released as water. In contrast, the ubiquitous flavin-dependent oxidases use O_2 as a two-electron, two-proton acceptor to produce H_2O_2. A transient C4a-hydroperoxyflavin species has been established by spectroscopic methods in *p*-hydroxybenzoate 3-hydroxylase (*3*), *p*-hydroxyphenylacetate 3-hydroxylase (*4*), luciferase (*5*), and microsomal flavin-containing monooxygenase (*6*). A similar species has also been detected in oxidases via rapid kinetic studies of pyranose 2-oxidase (*7*), on a mutant form of NADH oxidase (*8*), and pulse radiolysis experiments with

[†] This work was supported in part by a grant from the American Chemical Society Petroleum Research Fund (40310-G4), an American Heart Association Grant in Aid (0555286B), the Offices of Biological and Environmental Research of the U.S. Department of Energy, and the National Institutes of Health (2 P41 RR012408) to A.M.O.; an NSF CAREER Award (MCB-0545712), a grant from the American Chemical Society Petroleum Research Fund (37351-G4), and a Georgia State University Research Initiation Grant to G.G.; a Molecular Basis Disease Fellowship from Georgia State University to S.F.; and a U.S. Department of Education GAANN Fellowship to G.T.L.

[‡] The atomic coordinates and structure factors have been deposited in the Protein Data Bank as entry 2jbv.

* To whom correspondence should be addressed. A.M.O.: e-mail, amorv@bnl.gov; phone, (631) 344-4739; fax, (631) 344-2741. G.G.: e-mail, ggadda@gsu.edu; phone, (404) 413-5537; fax, (404) 413-5505. R.P.: e-mail, rpr@miami.edu; phone, (305) 284-9372; fax, (305) 284-1880.

[§] Brookhaven National Laboratory.

[||] Georgia Institute of Technology.

[⊥] Current address: Macromolecular Crystallography Laboratory, Center for Cancer Research, National Cancer Institute at Frederick, Frederick, MD 21702-1201.

[#] Department of Chemistry, Georgia State University.

[+] Department of Biology and The Center for Biotechnology and Drug Design, Georgia State University.

[▽] University of Miami.

10.1021/bi801918u CCC: $40.75
Published on Web 01/09/2009

glucose oxidase (*9*). Because a C4a−oxygen adduct is so rarely observed in oxidases, some authors recently proposed that flavin reoxidation in these enzymes proceeds preferentially by an outer-sphere electron transfer process, rather than through formation of a C4a−hydroperoxide intermediate (*10*). Regardless of the mechanism or enzyme family classification, to date there is no structurally defined flavin C4a−oxygen adduct in the Protein Data Bank.

Choline oxidase (EC 1.1.3.17; choline-oxygen 1-oxidoreductase) from *Arthrobacter globiformis* catalyzes the four-electron oxidation of choline to glycine betaine (*N*,*N*,*N*-trimethylglycine) via two sequential, FAD-dependent reactions in which betaine aldehyde is formed as an obligatory enzyme-bound intermediate (*11*). In each of the oxidative half-reactions, a molecule of O_2 is converted into H_2O_2. The midpoint reduction potentials for the FAD in choline oxidase are 211 ± 2 and −65 ± 2 mV for the FAD−FAD^{sq} and FAD^{sq}−$FADH^-$ couples, respectively (*12*). These values are among the highest determined to date for any flavoprotein and are thought to be influenced by several active site characteristics, including a covalent linkage between the C8M position and His99. We recently determined the crystal structure of choline oxidase at 1.86 Å resolution under cryogenic conditions (*13*). A novel but unexplained feature of the structure is the flavin cofactor, which exhibits a distorted isoalloxazine ring system and suggests the presence of a novel C4a adduct. In this report, we provide evidence strongly suggesting that a C4a−OH or C4a−OO(H) adduct forms in an X-ray-dependent process under cryogenic conditions. The essential insights derive from single-crystal microspectrophotometry concurrent with X-ray diffraction collected recently at the new single-crystal spectroscopy facility located at the National Synchrotron Light Source (see the Supporting Information and Figure S1), which is now available on a full-time basis to the general user population. The spectroscopic data also correlate very well with density functional theory (DFT)[1] calculations and the high-resolution X-ray crystal structure of the enzyme.

MATERIALS AND METHODS

Enzyme Purification, Crystallization, Structure Determination, and Model Refinement. Oxidized choline oxidase from *A. globiformis* strain ATCC 8010 was expressed from pET/codA in *Escherichia coli* and purified to homogeneity as described previously (*13*−*15*). Crystals of choline oxidase were grown aerobically by hanging drop vapor diffusion from 1.2−1.8 M ammonium sulfate and 10% (v/v) dimethyl sulfoxide (DMSO) in 0.1 M Bis-Tris propane (pH 8.5). Single crystals were transferred from the mother liquor into a cryoprotectant solution consisting of 3.4 M sodium malonate (pH 7.0) and allowed to soak for 2 min prior to being flash-frozen in liquid nitrogen (*13*). Several independent crystals were used for X-ray diffraction data sets and for single-crystal microspectrophotometry. X-ray diffraction data were collected at either the SER-CAT facilities (22-ID and 22-BM) at the Advanced Photon Source at Argonne National Laboratory or beamline X12-B, X25, X26-C, or X29 of the National Synchrotron Light Source at Brookhaven National Laboratory. The crystal structure was determined by molecular replacement as previously described (*13*) using the coordinates of the crystal structure of glucose oxidase [PDB entry 1CF3 (*16*)] as a search model. Choline oxidase crystallizes with one homodimer in the asymmetric unit in space group $P4_32_12$ with the following unit cell dimensions: $a = b = 84.4$ Å, and $c = 343.5$ Å. The high-resolution data set extends to a resolution of 1.86 Å. Crystals of aerobic choline oxidase were also grown from 1.2−1.8 M ammonium sulfate and 10% (v/v) 1,4-dioxane in 0.1 M Bis-Tris propane (pH 8.5). These conditions yield crystals in space group $P2_1$ with four homodimer enzymes in the asymmetric unit and typical unit cell dimensions: $a = 69.3$ Å, $b = 346.2$ Å, $c = 105.9$ Å, and $\beta = 94.3°$.

Refinements and model adjustments for the active site FAD were carried out as previously described (*13*). All library files with restraints were prepared using the PRODRG server (http://davapc1.bioch.dundee.ac.uk/programs/prodrg/). Initially, the FAD was refined using restraints to confer planarity on the entire isoalloxazine ring. Electron density maps at this point clearly revealed significant bending of the pyrimidine ring, and the $mF_o - DF_c$ maps contoured at 3σ returned negative features on the flat pyrimidine ring and a lobe of positive difference density that protruded from the C4a position and the pyrimidine ring. The isoalloxazine was then manually adjusted to properly fit the pyrimidine ring into the electron density; the restraints were adjusted to remove planar restraints from the pyrimidine ring, and sp^3 hybridization was conferred upon the C4a atom. Planar restraints were applied to the dimethylbenzene ring and the atoms of the piperazine ring. Electron density maps from the refinement indicated a good fit of the pyrimidine ring at this point, but the $mF_o - DF_c$ maps revealed $>4\sigma$ positive difference features near the C4a atom. At this point, two series of refinements were performed. In one round, the sp^3 C4a atom was bonded to a single oxygen atom (FAD C4a−O^-), and the model was refined. An FAD C4a−O_2^- model was also refined. The resulting maps indicated that the O_2 moiety also fits the $2mF_o - DF_c$ maps quite well; however, the occupancy of the distal oxygen atom refined best with an occupancy value of 0.5. To check for model bias, $2mF_o - DF_c$ and $mF_o - DF_c$ simulated annealing omit maps were prepared in CNS. The FAD, DMSO, residues His99 and His466, and all atoms within a 3.5 Å radius were removed from the model. The simulated annealing and map calculation was carried out with a starting temperature of 1000 K with data from 50.0 to 1.86 Å resolution.

Two additional models were also refined with *REFMAC5*. The first included a water molecule centered in the difference peak and unrestrained with respect to the FAD C4a atom. Upon convergence of the refinement of this model, the water molecule was only 1.6 Å from the C4a atom (Table S1 of the Supporting Information), and there was continuous electron density between the two atoms. However, since there is no H_2O−C4a bond, this model does not satisfy the observed sp^3 hybridization of the flavin C4a atom. The

[1] Abbreviations: flavin C4a−OO(H), C4a−hydroperoxyflavin species; C4a−O_p−O_d, proximal and distal atoms in the C4a−hydroperoxy species; C4a−OH, C4a−hydroxyflavin species; FAD^{sq}, one-electron-reduced flavin semiquinone; DMSO, dimethyl sulfoxide; $FADH^-$, two-electron-reduced, anionic flavin species; DFT, density functional theory.

second alternative model consisted of a covalent FAD C4a−OH moiety, which refined to a bond distance of 1.45 Å.

Single-Crystal Microspectrophotometry. We built a single-crystal μ-spectroscopy facility (SCμSF) at beamline X26-C at the National Synchrotron Light Source at Brookhaven National Laboratory for use by the general user population (see Figure S1 of the Supporting Information). The microspectrophotometer components were from a 4DX-ray Systems AB apparatus. We adapted it so that the microscopic optical axis and focal points were aligned with the crystal rotation axes of the diffractometer and X-ray beam at beamline X26-C. The microscope objectives used parabolic mirrors to achieve a magnification of 15× and to minimize spherical or chromatic aberration in the wavelength range from approximately 150 to 10000 nm. The objectives provide a 24 mm working distance through a 0.4 numerical aperture, which allows for cryocooling and access for other microspectroscopic components. When coupled with a 50 μm quartz optical fiber, the incident spot size is approximately 25 μm in diameter. The transmitted light is collected from a spot approximately 75 μm in diameter. The incident light (350−850 nm) was from a 75 W Xe research arc lamp (Newport Corp.). An Ocean Optics (Dunedin, FL) USB 4000 spectrophotometer containing a 3648-element Toshiba linear CCD detector was used to collect the optical absorption spectra. The data were processed initially with SpectraSuit on either a Windows XP or LINUX operating system. The spectrophotometer was calibrated and microspectroscopically aligned with a Hg−Ar calibration laser. Typically, optical absorption spectra were collected by averaging 10 spectra, each of which was collected with an integration time of approximately 70 ms and a 10-pixel "box car" of the CCD detector array. Crystals were held at 100 K during X-ray diffraction and optical absorption spectroscopic data collection.

Computational Procedures. All calculations were performed using Gaussian 03 (*17*). The geometries of all the structures were optimized without any symmetry constraints using the DFT-based B3LYP method with the 6-31G(d) basis set in the gas phase (*18*−*20*). The final energies were calculated using a large 6-31+G(d,p) basis set including diffuse and polarization functions. Since it was computationally unfeasible to calculate unscaled zero-point energy and thermal corrections on the large models used in this study, they were not included. The dielectric effects (for $\varepsilon = 4.3$) from the surrounding protein were incorporated using the self-consistent reaction field method (*21*) at the B3LYP/(6-31G(d)) level. To retain the steric effect of the surrounding protein, one hydrogen atom each in the backbones of His351 and His466 was kept frozen from the X-ray structure. This kind of approach is known to preserve some of the steric effect of the protein surroundings (*22*). The remaining degrees of freedom of all the structures were optimized. The initial models used in the DFT calculations were extracted from the crystal structure. Rather large models were used in the calculations (ca. 180 atoms) and included the FAD and active site residues His99, Asn100, Ser101, DMSO, Ile103, His351, His466, Asn510, and Pro511. The backbone atoms of residues His351 and His466 and the ribityl side chain of the FAD were omitted from the calculation.

RESULTS AND DISCUSSION

To investigate the single-crystal spectroscopic properties of choline oxidase as a function of X-ray exposure, we harvested yellow crystals of the oxidized enzyme from aerobic mother liquor. After crystals had been transferred to a cryoprotectant (3.5 M sodium malonate), they were individually mounted in nylon loops and flash-cooled by being plunged into liquid N_2. We performed several types of experiments with enzyme crystallized in space group $P4_32_12$ or $P2_1$ from ammonium sulfate. The exposure to 1 Å (12.398 KeV) X-ray photons ($\sim 4 \times 10^{10}$ photons/s through a 200 μm diameter collimated beam) at 100 K was performed on stationary crystals or with crystals rotated through 180° at beamline X26-C of the National Synchrotron Light Source. The results are very reproducible, and typical spectra are shown in Figure 1. The absorption spectrum of choline oxidase crystals at 100 K prior to X-ray exposure reveals two maxima centered at 460 and 485 nm. We and others have observed that single-crystal spectra at low temperatures are anisotropic and depend critically on crystal orientation, especially when planar chromophores such as flavins are present within the crystal (*23, 24*). For example, AMO has collected single-crystal spectra from several oxidized flavoenzymes (data not shown), including nitroalkane oxidase, xenobiotic reductase A, cholesterol oxidase, and thioredoxin reductase, which all yield two resolved peaks near 450 nm. In most of these flavoenzymes and in choline oxidase in particular, the two maxima at 460 and 485 nm move up and down along with baseline excursions, as well as a change in their relative intensities with respect to each other as a function of the rotation angle. Thus, the single-crystal spectra of choline oxidase are better resolved than for the enzyme in solution at 300 K (for a typical example, see Figure S2 of the Supporting Information), which yields a peak at 450 nm and a shoulder at ~480 nm. After X-ray diffraction data collection, the optical spectrum of choline oxidase crystals yields a single absorption peak at approximately 400 nm. The difference spectra (after − before) clearly show an absorption band with a λ_{max} at 400 nm and features that extend from ~510 nm to longer wavelengths. The 400 nm feature represents the vast majority of the flavin species present in the region of the crystal exposed to X-rays and is remarkably similar to spectra obtained from transient flavin C4a−OO(H) or C4a−OH intermediates (*3*−*8*). For example, these types of C4a adducts typically have a maximum absorbance at ~380 nm; however, in low-temperature single crystals of choline oxidase, the absorbance spectrum for the C4a adduct is red-shifted approximately 20 nm. The longer wavelength features at 510 nm indicate that a small fraction of the enzyme contains a FAD semiquinone species as previously observed for choline oxidase in solution (*25*).

We next evaluated the time-dependent process of adduct formation in a single crystal at 100 K. Spectra were collected every 10 s from a stationary crystal of choline oxidase during exposure to the monochromatic synchrotron X-ray beam at X26-C. As illustrated in panels B and C of Figure 1, the difference feature at 400 nm increases in an exponential process with a $t_{1/2}$ of approximately 40 s. Thus, the

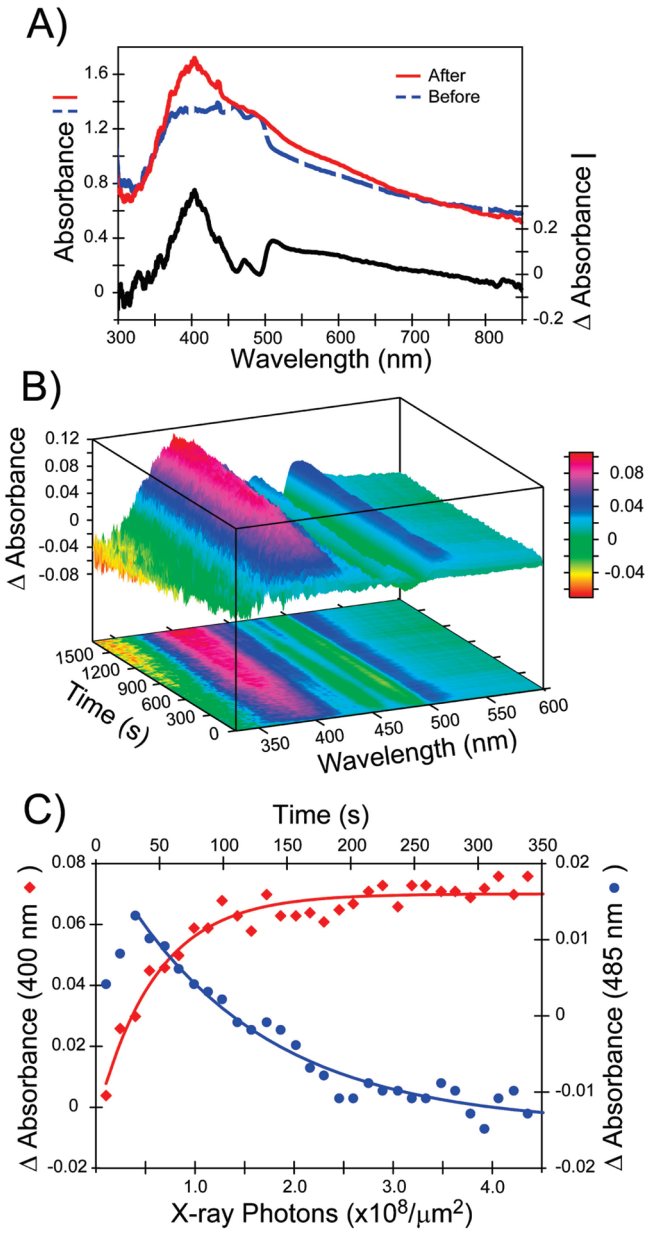

FIGURE 1: Spectroscopic changes observed in single crystals of choline oxidase upon X-ray irradiation at 100 K. (A) Optical spectra measured from a single crystal of choline oxidase before (blue) or after (red) an X-ray diffraction data set was collected with 180° of ϕ axis rotation. The difference between the two is shown with the black line and with the scale on the right. Each spectrum was recorded with the ϕ axis at 0° by averaging 10 spectra obtained with a 70 ms integration time and the box-car set to 10 pixel CCD elements. (B) Time-dependent change in the optical absorption spectrum of another choline oxidase crystal held stationary in the X-ray beam. Spectra were recoded every 10 s with the instrument parameters given for panel A. Six reference spectra were recoded before the X-ray shutter was opened, averaged, and then subtracted from each spectrum obtained after the X-ray shutter was opened. The bottom panel of the three-dimensional plot is a projection of the time-dependent difference spectra. (C) Difference features at 400 and 485 nm from panel B were fit to the single-exponential equation $y = ae^{bt} + c$, where t is the time in seconds and for the 400 nm data points $a = -0.074012$, $b = 0.021617$, and $c = 0.070048$, whereas the first two data points were excluded for the 485 nm and fit with $a = 0.036755$, $b = 0.0087557$, and $c = -0.0144$.

appearance of the spectral feature at 400 nm is nearly complete within the time required to collect only a small fraction of the unique X-ray diffraction data (equivalent to <10° of crystal rotation), even at the relatively modest X-ray intensity of beamline X26-C of the NSLS.[2] This process is also approximately commensurate with the decrease in the 460 and 485 nm features attributed to oxidized FAD [$t_{1/2}$ of approximately 100 s (Figure 1C)]. Optical spectra from enzyme in solution at room temperature show that the flavin semiquinone species (i.e., one-electron-reduced) has a spectrum that overlaps that of oxidized FAD (*25*). In contrast, the hydroquinone FAD species (i.e., reduced by two electrons) or the C4a adduct observed here has very little absorbance in the 450−500 nm region. Consequently, the exponential decay seen at 485 nm appears to be slower than the observed rate of formation of the 400 nm feature assigned to the C4a adduct. Taken together, the spectroscopic analyses of single crystals at low temperatures show that the decrease in the concentration of oxidized FAD in the region of the crystal exposed to X-rays is correlated to an increase of the concentration of the C4a adduct.

The atomic structure and 1.86 Å resolution simulated annealing omit electron density maps for the FAD are shown in Figure 2. The flavin isoalloxazine ring is not planar, as anticipated for oxidized choline oxidase, or bent along the N5−N10 axis as is often observed in reduced flavoproteins (*26*). The electron density for the dimethylbenzene and piperazine rings indicates that each ring is flat and coplanar with one another. However, the plane of the pyrimidine ring is at an approximately 120° angle to the plane of the other two rings (Table S1 of the Supporting Information). The electron density for the pyrimidine ring indicates that it adopts a "half-boat" configuration in which the C4a atom is approximately 0.5 Å above the pyrimidine ring plane. Moreover, throughout the refinement process, a $>4\sigma$ positive difference peak associated with the C4a atom persisted. This feature clearly indicates that the C4a atom is sp^3 hybridized and, therefore, that a covalent flavin adduct is present in the crystal structure. The electron density for the difference feature is large enough to accommodate only one or possibly two atoms in a covalently linked FAD C4a adduct.

To the best of our knowledge, the materials and aerobic crystallization conditions do not include any reagents that can readily form a C4a adduct with oxidized FAD. Moreover, none of the reagents used to crystallize the enzyme alter the optical spectrum of oxidized choline oxidase, indicating that the reagents do not perturb significantly the FAD electronic environment (see Figure S2 of the Supporting Information). In contrast, reduced flavins in the semiquinone or hydroquinone states do react with O_2 and can form C4a−oxygen adducts (*2, 9*). Therefore, we followed a conservative approach and refined a FAD C4a−OH atomic model, which converged well with *REFMAC5* to yield a C4a−O bond distance of 1.45 Å (Figure 2A and Table S1 of the Supporting Information). Next we modeled an O_2 molecule bound to the C4a atom of reduced FAD. After refinement with *REFMAC5*, the C4a−O_p and O_p−O_d bond lengths are 1.4 Å (Figure 2B and Table S1 of the Supporting Information) with a C4a−O_p−O_d bond angle of 116°. Although the estimated

[2] We believe that the spectroscopic alterations we observe as a function of X-ray exposure are not simply related to the intensity of the synchrotron X-ray beam, but also to the total dose absorbed by the crystal during data collection and the active site environment. Therefore, the chemistry and X-ray dose dependence of adduct formation are rather complex and are currently under further investigation.

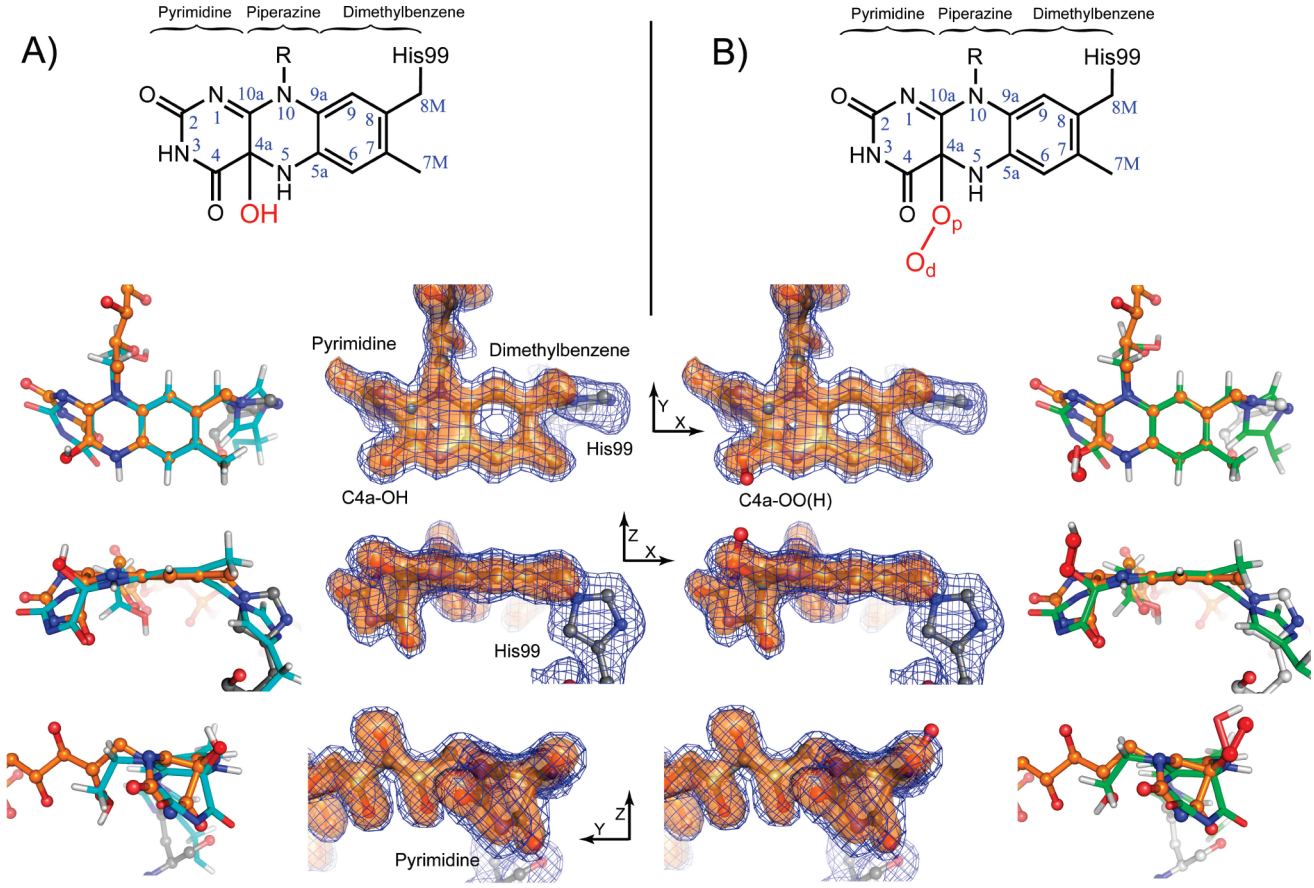

FIGURE 2: Comparison of the X-ray structures with the DFT-optimized models for the FAD C4a−OH adduct (A) or the C4a−OO(H) adduct (B). Orthogonal views of the simulated annealing omit electron density maps (50−1.86 Å resolution) for the FAD isoalloxazine ring in choline oxidase (bottom central portions). The $mF_o - DF_c$ difference map ($+3\sigma$) is shown with orange, translucent surface contours, and the $2mF_o - DF_c$ map (1σ) is displayed as a blue mesh. The FAD, C4a adduct, and DMSO were omitted from the model. For comparison, the refined C4a−OH and C4a−OO(H) atomic models are shown superimposed with C, N, and O atoms colored gray, blue, and red, respectively. The arrows labeled X, Y, and Z indicate the relative orientation of each image. An overlay of the X-ray structures with the DFT-optimized models for the FAD C4a−OH adduct and the C4a−OO(H) adduct (bottom outer portions). The refined crystal structure is shown with flavin C atoms and bonds colored orange superimposed with the DFT-optimized C4a−OH (C atoms rendered with cyan sticks) or C4a−OO(H) model (C atoms rendered with green sticks).

coordinate error of the model is approximately 0.1 Å, these parameters agree well with those determined by quantum mechanical calculations for the model FAD−C4a−OO(H) intermediate in *p*-hydroxybenzoate 3-hydroxylase and phenol hydroxylase (*27, 28*), as well as the DFT calculations discussed below. Therefore, the C4a−OH and C4a−OO(H) models for the FAD adduct in choline oxidase have reasonable geometry for sp^3 hybridization and the appropriate bond lengths and angles for a C4a adduct. However, the observed electron density for the distal oxygen atom (O_d) is weaker than for the proximal atom oxygen (O_p), and consequently, the former atom also has a higher *B* factor. This suggests that either the O_d atom may be partially disordered, possibly due to precession about the C4a−O_p bond, or only one oxygen atom is present in the adduct.

The simulated annealing omit maps provide the most unbiased view of the FAD adduct. During this procedure, the FAD, DMSO, and C4a adduct were omitted from the model. The resulting $mF_o - DF_c$ and $2mF_o - DF_c$ electron density maps (Figure 2A,B) calculated with reflections between 50 and 1.86 Å resolution were superimposed with refined models containing either the C4a−OH or the C4a−OO(H) adduct. This analysis prompts us to conclude that the FAD in choline oxidase is most likely a C4a−OH (hydroxy) flavin adduct. However, as discussed above, we cannot unambiguously rule out the C4a−OO(H) (peroxy or hydroperoxy) adduct. The resolution of the structure, the quality of the refined atomic models, and the fits to the observed electron density for choline oxidase are comparable to those of the recently reported dioxygen complexes of cytochrome $P450_{cam}$ (*29*), naphthalene dioxygenase (*30*), superoxide reductase (*31*), homoprotocatechuate 2,3-dioxygenase (*32*), and amine oxidase (*33*).

The X-ray crystal structure shows that the active sites are completely sequestered within each subunit of the dimeric enzyme such that there is no direct access of bulk solvent to the FAD isoalloxazine ring. Nevertheless, a DMSO molecule, an additive in the crystallization solution, is observed in the solvent-excluded cavity within each active site (Figure S3 of the Supporting Information). In addition to the covalent bond between the dimethylbenzene ring and His99, several deduced hydrogen bonds stabilize the isoalloxazine ring configuration and the C4a−OH [or C4a−OO(H)] adduct. For example, the FAD pyrimidine ring forms a network of hydrogen bonds with protein backbone atoms from Asn100, Cys102, Ile103, and Asn512. In addition, there are side chain interactions between the pyrimidine ring and Asn100 and Ser101. Consequently, nearly every atom of the isoalloxazine

ring in this unusual configuration with the potential to participate in hydrogen bonds does so with either a protein residue[3] or the DMSO. Furthermore, the structure indicates that the atoms of either C4a adduct are stabilized by hydrogen bonds with the side chains of His351 and Asn510. Finally, the DMSO molecule is located adjacent to the C4a adduct and also hydrogen bonds with the side chain of Ser101 and the FAD N5 moiety.

To gain a better understanding of the electronic structure of the unique isoalloxazine ring configuration observed in the X-ray structure of choline oxidase, we performed a number of DFT calculations. Each structure was optimized using Gaussian 03 (*17*) at the B3LYP/6-31G(d) level in the gas phase. The final energies were calculated using a large 6-31+G(d,p) basis set, which included dielectric effects (for $\varepsilon = 4.3$) from the surrounding protein using the self-consistent reaction field (IEFPCM) method at the B3LYP/6-31G(d) level. The largest calculations (ca. 180 atoms) included the FAD isoalloxazine ring and most of the first-shell residues comprising the active site (see Figure S3 of the Supporting Information; His99, Asn100, Ser101, Cys102, Ile103, His310, His351, His466, Asn510, Pro511, Asn512, and a DMSO molecule). Several flavin electronic states within the enzyme active site were computed, including (a) one-electron-reduced flavin semiquinone (FAD^{sq}), (b) a reduced flavin C4a−hydroperoxy complex [FAD C4a−OO(H)], (c) a flavin C4a−hydroxy complex (FAD C4a−OH), and (d) a flavin C4a−peroxy complex (FAD C4a−OO^-). The metrics for the observed X-ray structure and the DFT-optimized structures for each flavin species are summarized in Table S1 of the Supporting Information.

The DFT calculations unequivocally indicate that formation of the FAD C4a adduct and the first-shell hydrogen bond interactions with the flavin moiety are both necessary to reproduce the observed X-ray structure (Figure 2 and Figures S3 and S4 of the Supporting Information). Unfortunately, the accuracy of the DFT calculations and the uncertainty of the crystal structure do not support a clear discrimination between the C4a−OH and C4a−OO(H) structures. In contrast, gas phase optimizations of protein-free flavin adducts yield less distorted FAD C4a−OO(H) and FAD C4a−OH structures (Figure S4D of the Supporting Information). By comparison of these structures, we estimate that the energies required to stabilize the X-ray structure of the enzyme are ∼29 kcal/mol for the FAD C4a−OH adduct and 22 kcal/mol for the FAD C4a−OO(H) adduct. Either of these total energetic contributions that stabilize the distorted flavin C4a adduct is consistent with the crystal structure and the numerous active site hydrogen bonds deduced between the distorted FAD and active site residues. In this context, our computational analysis suggests that the hydrogen bonding interactions of the flavin with the side chains of His99, Asn100, Ser101, Cys102, Ile103, Asn510, His466, and His351 (Figure S3 of the Supporting Information) are essential for the stabilization of the distorted flavin C4a adduct. This is underscored by our additional computations (not shown) suggesting that removal of any of these residues in silico yields a more planar flavin C4a adduct.

[3] In contrast, preliminary X-ray diffraction and structural analysis of an active site mutant of CHO where Ser101 was replaced with alanine does not yield an adduct with conditions that do form the adduct in the wild-type CHO.

We also considered alternative scenarios, including degradation of the isoalloxazine ring system similar to that reported by Iwata et al. (*34*), but in this case being initiated by reduction of the flavin in the X-ray beam. Indeed, due to the formation of the C4a=O bond, some of the DFT-optimized models resulted in ring-open products similar to the 10a-spirohydantoin characterized by Iwata. However, we ruled out this hypothesis on the basis of structural and spectroscopic evidence. First, our high-resolution electron density maps are of sufficient quality to establish sp^3 and sp^2 hybridization at the flavin C4a and C10a atoms, respectively. In contrast, the best-characterized 10a-spirohydantoin degradation product has sp^3 and sp^2 hybridization at atoms analogous to flavin C10a and C4a, respectively. Our single-crystal spectroscopic analysis also supports the C4a adduct. Indeed, while the optical spectrum for the choline oxidase adduct has a λ_{max} near 400 nm, the optical spectrum for the degradation products mentioned by Iwata has a λ_{max} near 310 nm.

Solvated electrons are generated in biological samples by synchrotron X-ray irradiation on the time scale of electronic transitions (see, for example, ref *35* and references cited therein). Rapid electron transfer over significant distances can be facilitated by aromatic side chains, protein backbone atoms, and protein secondary structure (*36*). Consequently, it is very likely that the FAD in choline oxidase is reduced in the X-ray beam. We propose that the high reduction potential for the enzyme-bound FAD provides a strong thermodynamic driving force for capturing the solvated electrons (Figure 3, path a). This conclusion is consistent with the negative features observed in the difference spectra at 450 and 480 nm, as well as the 510 nm features ascribed to the FAD semiquinone as a minor but persistent species. Our DFT calculations indicate that the unpaired electron in an anionic FAD semiquinone radical, which is stabilized in choline oxidase, is delocalized among the C4a (0.19e), C9 (0.18e), C7 (0.08e), C8 (−0.13e), and C8 M (0.58e) atoms of the isoalloxazine ring system. Thus, the spectroscopic results show that the exposure of the crystal to the X-ray beam at low temperatures is commensurate with a decrease in concentration of oxidized FAD in the sample.

Hydroxyl and superoxide radicals, as well as other reaction products, are also generated in biological samples by X-ray exposure, but on a time scale of microseconds to milliseconds (*35*). However, the migration of hydroxyl and superoxide radicals, dioxygen, and protons within proteins at cryogenic temperatures is less well understood than electron transfer processes. Nevertheless, this raises the possibility that the C4a adduct may form by one of several scenarios, which differ principally in the origin of the oxygen atom in the C4a adduct (Figure 3). For example, our DFT calculations show that a hydroxyl radical does react with the C4a position of a FAD semiquinone yielding a flavin C4a−OH species, but only if the two radicals are near each other (ca. 2.0−2.2 Å and only if the flavin N5 atom is unprotonated (Figure 3, path b). Similarly, our calculations indicate that a reaction between superoxide radical and the FAD semiquinone yielding a flavin C4a−OO(H) species is also possible (Figure 3, path c). Alternatively, the C4a−OO(H) adduct may derive from a reaction between a two-electron-reduced flavin ($FADH^-$) and a ground-state O_2 (Figure 3, path d). Previous experimental and theoretical studies have demonstrated that

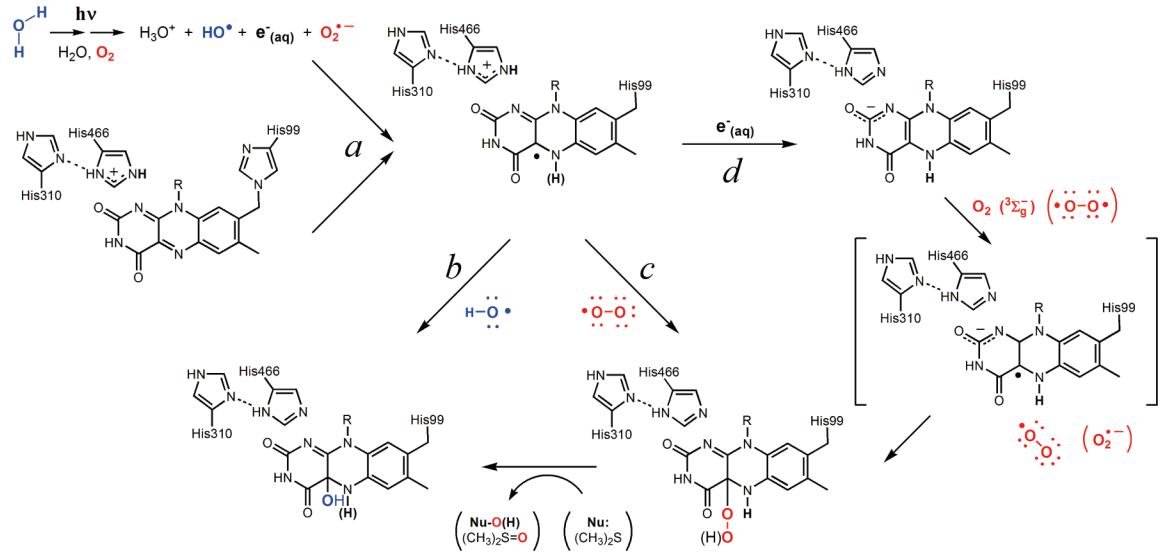

FIGURE 3: Proposed reaction scheme for formation of the C4a adduct in single crystals of choline oxidase at 100 K. Radiolysis of solvent by X-rays yields solvated electrons and several types of reactive oxygen species (path a). An electron migrates to the high-reduction potential FAD within the active site to yield the flavin semiquinone (path a). Either a hydroxyl radical (path b) or a superoxide radical (path c) then combines with the flavin semiquinone to form the C4a−OH or C4a−OO(H) species, respectively. It is also possible to form the C4a−OO(H) species via two-electron reduction of the flavin, followed by reaction with O_2 (path d). Reaction of the flavin C4a−OO(H) species with an appropriate nucleophile (Nu:), such as dimethyl sulfide, can also yield the C4a−OH adduct.

a flavin radical can react with dimethyl sulfide to yield a flavin C4a−OH adduct and DMSO (*37, 38*). Our crystallization conditions include 10% (v/v) DMSO, which likely has dimethyl sulfide as a minor contaminant component. Consequently, a trace amount of dimethyl sulfide could promote conversion of the semiquinone to yield the C4a−OH adduct, but in this case, the resulting oxygen atom in the observed adduct originates from O_2 rather than solvent. Each of the scenarios presented here requires that for a C4a adduct to form, the appropriate reactants (with the exception of solvated electrons) must be either present or generated in the vicinity of the flavin isoalloxazine ring. Indeed, diffusion of bulky species over long distances or through the protein and/or crystal matrix to the interior FAD C4a position is very unlikely at 100 K. In contrast, the proposed short-range migration of radical species or ground-state O_2 within the choline oxidase active site is analogous to the well-documented results of carbon monoxide photodissociation of myoglobin−CO complexes (*39, 40*).

Irrespective of the mechanism of formation of the flavin C4a−OH or C4a−OO(H) adduct, it seems likely that once formed neither breaks down to release water or H_2O_2 because the cryogenic conditions do not establish the correct proton inventory on the surrounding residues and the flavin to facilitate product dissociation.[4] In contrast, during catalytic turnover with choline (*11*), the enzyme coordinates the extraction of two protons and two electrons from the substrate with their subsequent delivery to O_2 to yield H_2O_2 (see Figure S5 of the Supporting Information). Indeed, during the reductive half-reaction, the net transfer and storage of two proton equivalents from the substrate to the active site base and the flavin N5 atom is commensurate with the two-electron reduction of the flavin. In the subsequent oxidative half-reaction, the two electrons are transferred from the reduced flavin to O_2 along with the delivery of the two stored protons. Therefore, an incorrect proton inventory on the active site residues may stall the oxidative half-reaction. Thus, the X-ray exposure at low temperatures creates an improper proton inventory scenario that consequently yields the structure of choline oxidase containing the C4a adduct.

To date, we have not obtained evidence for a similar C4a adduct species in choline oxidase in experiments conducted in solution. However, very recently, Sucharitakul et al. reported that pyranose 2-oxidase from *Trametes multicolor* does form a transient C4a−hydroperoxyflavin intermediate in its oxidative half-reaction. Moreover, that enzyme exhibits spectroscopic characteristics for the C4a adduct in solution that are very similar to those of the adduct we observe in single crystals of choline oxidase. In addition, the pyranose 2-oxidase from *T. multicolor* (*41*−*44*) is structurally related to choline oxidase and other members of the glucose-methanol-choline (GMC) oxidoreductase enzyme superfamily that catalyze the oxidation of alcohols.

Flavoenzyme mechanistic schemes often invoke FAD C4a−OO(H) or C4a−OH intermediates, but they have heretofore eluded structural characterization and have only rarely been detected by transient kinetic and spectroscopic techniques (*1, 2, 9*). However, the structural environment in the active site of choline oxidase appears to be ideally suited to stabilize a C4a adduct involving an oxygen species. This study is therefore the first direct observation by X-ray crystallography of a hydroxyflavin or peroxoflavin intermediate in any flavoenzyme, despite decades of effort by many researchers in the field, and numerous mechanistic proposals that invoke such a species. Our multidisciplinary experimental approach and correlation with complementary theoretical analysis thus provide direct evidence for an important oxygen intermediate in the reaction cycle of flavin-dependent enzymes.

[4] To date, we have not been able to determine cryo-conditions that allow us to thaw crystals after X-ray exposure and then permit us to use them for additional low-temperature spectroscopic and diffraction studies.

ACKNOWLEDGMENT

Data for this study were measured, in part, at beamlines X12B, X25, X26-C, and X29 of the National Synchrotron Light Source, Brookhaven National Laboratory. Use of the National Synchrotron Light Source at Brookhaven National Laboratory was supported by the U.S. Department of Energy Office of Basic Energy Sciences, under Contract DE-AC02-98CH10886. Some of the X-ray diffraction data were also collected at Southeast Regional Collaborative Access Team (SER-CAT) beamlines 22-ID and 22-BM at the Advanced Photon Source (APS), Argonne National Laboratory (SER-CAT supporting institutions may be found at http://www.ser-cat.org/members.html). Use of the Advanced Photon Source was supported by the U.S. Department of Energy, Office of Science, Office of Basic Energy Sciences, under Contract W-31-109-Eng-38. We thank the SER-CAT staff at APS for assistance during data collection and Dr. Zhongmin Jin for assistance with the mail-in crystallography program. We are also grateful to the PXRR scientific staff at BNL for many helpful discussions, to Mr. Matt Cowan for assistance with the analysis and plotting of the time-dependent spectroscopic data of choline oxidase crystals, and to Ms. Mary Carlucci-Dayton for engineering and design assistance to mount the microspectrophotometer to beamline X26-C.

SUPPORTING INFORMATION AVAILABLE

Selected bond distances and angles in the X-ray structure and DFT-optimized models (Table S1), single-crystal optical absorption spectroscopy facility installed at beamline X26-C at the NSLS (Figure S1), optical absorption spectrum of choline oxidase in solution, at room temperature, and with all the crystallization reagents added (Figure S2), active site environment of choline oxidase illustrating the potential hydrogen bonding interactions that stabilize the C4a adduct (Figure S3), an overlay of several DFT-optimized C4a adducts and the crystal structure of choline oxidase (Figure S4), proposed reaction mechanism for choline oxidase (Figure S5), and coordinates for several DFT-optimized FAD C4a adducts in X, Y, Z, and PDB formats. This material is available free of charge via the Internet at http://pubs.acs.org.

REFERENCES

1. Massey, V. (2000) The chemical and biological versatility of riboflavin. *Biochem. Soc. Trans. 28*, 283–296.
2. Mattevi, A. (2006) To be or not to be an oxidase: Challenging the oxygen reactivity of flavoenzymes. *Trends Biochem. Sci. 31*, 276–283.
3. Entsch, B., Ballou, D. P., and Massey, V. (1976) Flavin-oxygen derivatives involved in hydroxylation by *p*-hydroxybenzoate hydroxylase. *J. Biol. Chem. 251*, 2550–2563.
4. Sucharitakul, J., Chaiyen, P., Entsch, B., and Ballou, D. P. (2006) Kinetic mechanisms of the oxygenase from a two-component enzyme, p-hydroxyphenylacetate 3-hydroxylase from *Acinetobacter baumannii*. *J. Biol. Chem. 281*, 17044–17053.
5. Abu-Soud, H., Clark, A., Francisco, W., Baldwin, T., and Raushel, F. (1993) Kinetic destabilization of the hydroperoxy flavin intermediate by site-directed modification of the reactive thiol in bacterial luciferase. *J. Biol. Chem. 268*, 7699–7706.
6. Jones, K. C., and Ballou, D. P. (1986) Reactions of the 4a-hydroperoxide of liver microsomal flavin-containing monooxygenase with nucleophilic and electrophilic substrates. *J. Biol. Chem. 261*, 2553–2559.
7. Sucharitakul, J., Prongjit, M., Haltrich, D., and Chaiyen, P. (2008) Detection of a C4a-hydroperoxyflavin intermediate in the reaction of a flavoprotein oxidase. *Biochemistry 47*, 8485–8490.
8. Mallett, T. C., and Claiborne, A. (1998) Oxygen reactivity of an NADH oxidase C42S mutant: Evidence for a C(4a)-peroxyflavin intermediate and a rate-limiting conformational change. *Biochemistry 37*, 8790–8802.
9. Massey, V. (1994) Activation of molecular oxygen by flavins and flavoproteins. *J. Biol. Chem. 269*, 22459–22462.
10. Prabhakar, R., Siegbahn, P. E. M., Minaev, B. F., and Agren, H. (2002) Activation of triplet dioxygen by glucose oxidase: Spin-orbit coupling in the superoxide ion. *J. Phys. Chem. B 106*, 3742–3750.
11. Fan, F., and Gadda, G. (2005) On the catalytic mechanism of choline oxidase. *J. Am. Chem. Soc. 127*, 2067–2074.
12. Ghanem, M., and Gadda, G. (2006) Effects of reversing the protein positive charge in the proximity of the flavin N(1) locus of choline oxidase. *Biochemistry 45*, 3437–3447.
13. Quaye, O., Lountos, G. T., Fan, F., Orville, A. M., and Gadda, G. (2008) Role of Glu312 in Binding and Positioning of the Substrate for the Hydride Transfer Reaction in Choline Oxidase. *Biochemistry 47*, 243–256.
14. Fan, F., Ghanem, M., and Gadda, G. (2004) Cloning, sequence analysis, and purification of choline oxidase from *Arthrobacter globiformis*: A bacterial enzyme involved in osmotic stress tolerance. *Arch. Biochem. Biophys. 421*, 149–158.
15. Gadda, G., Powell, N. L., and Menon, P. (2004) The trimethylammonium headgroup of choline is a major determinant for substrate binding and specificity in choline oxidase. *Arch. Biochem. Biophys. 430*, 264–273.
16. Wohlfahrt, G., Witt, S., Hendle, J., Schomburg, D., Kalisz, H. M., and Hecht, H. J. (1999) 1.8 and 1.9 Å resolution structures of the *Penicillium amagasakiense* and *Aspergillus niger* glucose oxidases as a basis for modelling substrate complexes. *Acta Crystallogr. D55*, 969–977.
17. Frisch, M. J., Trucks, G. W., Schlegel, H. B., Scuseria, G. E., Robb, M. A., Cheeseman, J. R., Montgomery, J. A., Jr., Vreven, T., Kudin, K. N., Burant, J. C., Millam, J. M., Iyengar, S. S., Tomasi, J., Barone, V., Mennucci, B., Cossi, M., Scalmani, G., Rega, N., Petersson, G. A., Nakatsuji, H., Hada, M., Ehara, M., Toyota, K., Fukuda, R., Hasegawa, J., Ishida, M., Nakajima, T., Honda, Y., Kitao, O., Nakai, H., Klene, M., Li, X., Knox, J. E., Hratchian, H. P., Cross, J. B., Bakken, V., Adamo, C., Jaramillo, J., Gomperts, R., Stratmann, R. E., Yazyev, O., Austin, A. J., Cammi, R., Pomelli, C., Ochterski, J. W., Ayala, P. Y., Morokuma, K., Voth, G. A., Salvador, P., Dannenberg, J. J., Zakrzewski, V. G., Dapprich, S., Daniels, A. D., Strain, M. C., Farkas, O., Malick, D. K., Rabuck, A. D., Raghavachari, K., Foresman, J. B., Ortiz, J. V., Cui, Q., Baboul, A. G., Clifford, S., Cioslowski, J., Stefanov, B. B., Liu, G., Liashenko, A., Piskorz, P., Komaromi, I., Martin, R. L., Fox, D. J., Keith, T., Al-Laham, M. A., Peng, C. Y., Nanayakkara, A., Challacombe, M., Gill, P. M. W., Johnson, B., Chen, W., Wong, M. W., Gonzalez, C., and Pople, J. A. (2004) Gaussian 03, revision C1, Gaussian, Inc., Wallingford, CT.
18. Becke, A. D. (1988) Density-functional exchange-energy approximation with correct asymptotic behavior. *Phys. Rev. A 38*, 3098–3100.
19. Becke, A. D. (1993) Density-functional thermochemistry. III. The role of exact exchange. *J. Chem. Phys. 98*, 5648–5652.
20. Lee, C. T., Yang, W. T., and Parr, R. G. (1988) Development of the Colle-Salvetti correlation-energy formula into a functional of the electron-density. *Phys. Rev. B 37*, 785–789.
21. Cances, E., Mennucci, B., and Tomasi, J. (1997) A new integral equation formalism for the polarizable continuum model: Theoretical background and applications to isotropic and anisotropic dielectrics. *J. Chem. Phys. 107*, 3032–3041.
22. Prabhakar, R., Morokuma, K., and Musaev, D. G. (2005) A comparative study of various computational approaches in calculating the structure of pyridoxal 5′-phosphate (PLP)-dependent β-lyase protein. The importance of protein environment. *J. Comput. Chem. 26*, 443–446.
23. De la Mora-Rey, T., and Wilmot, C. M. (2007) Synergy within structural biology of single crystal optical spectroscopy and X-ray crystallography. *Curr. Opin. Struct. Biol. 17*, 580–586.
24. Siddiqui, M. S., and Stanley, R. J. (2005) A cryogenic optical waveguide spectrometer for the measurement of low-temperature absorption spectra of dilute biological samples. *Anal. Biochem. 337*, 121–129.
25. Ghanem, M., Fan, F., Francis, K., and Gadda, G. (2003) Spectroscopic and kinetic properties of recombinant choline oxidase from *Arthrobacter globiformis*. *Biochemistry 42*, 15179–15188.

26. Dixon, D. A., Lindner, D. L., Branchaud, B., and Lipscomb, W. N. (1979) Conformations and electronic structures of oxidized and reduced isoalloxazine. *Biochemistry 18*, 5770–5775.
27. Ridder, L., Harvey, J. N., Rietjens, I. M. C. M., Vervoort, J., and Mulholland, A. J. (2003) Ab initio QM/MM modeling of the hydroxylation step in p-hydroxybenzoate hydroxylase. *J. Phys. Chem. B 107*, 2118–2126.
28. Ridder, L., Mulholland, A. J., Rietjens, I. M. C. M., and Vervoort, J. (2000) A quantum mechanical/molecular mechanical study of the hydroxylation of phenol and halogenated derivatives by phenol hydroxylase. *J. Am. Chem. Soc. 122*, 8728–8738.
29. Schlichting, I., Berendzen, J., Chu, K., Stock, A. M., Maves, S. A., Benson, D. E., Sweet, R. M., Ringe, D., Petsko, G. A., and Sligar, S. G. (2000) The catalytic pathway of cytochrome p450cam at atomic resolution. *Science 287*, 1615–1622.
30. Karlsson, A., Parales, J. V., Parales, R. E., Gibson, D. T., Eklund, H., and Ramaswamy, S. (2003) Crystal structure of naphthalene dioxygenase: Side-on binding of dioxygen to iron. *Science 299*, 1039–1042.
31. Katona, G., Carpentier, P., Niviere, V., Amara, P., Adam, V., Ohana, J., Tsanov, N., and Bourgeois, D. (2007) Raman-assisted crystallography reveals end-on peroxide intermediates in a nonheme iron enzyme. *Science 316*, 449–453.
32. Kovaleva, E. G., and Lipscomb, J. D. (2007) Crystal structures of Fe^{2+} dioxygenase superoxo, alkylperoxo, and bound product intermediates. *Science 316*, 453–457.
33. Wilmot, C. M., Hajdu, J., McPherson, M. J., Knowles, P. F., and Phillips, S. E. (1999) Visualization of dioxygen bound to copper during enzyme catalysis. *Science 286*, 1724–1728.
34. Iwata, M., Bruice, T. C., Carrell, H. L., and Glusker, J. P. (1980) Reactions of 4a-peroxides and 4a-pseudobases of N10- and N5-phenethylflavins. *J. Am. Chem. Soc. 102*, 5036–5044.
35. Xu, G., and Chance, M. R. (2007) Hydroxyl radical-mediated modification of proteins as probes for structural proteomics. *Chem. Rev. 107*, 3514–3543.
36. Gray, H. B., and Winkler, J. R. (1996) Electron transfer in proteins. *Annu. Rev. Biochem. 65*, 537–561.
37. Kemal, C., Chan, T. W., and Bruice, T. C. (1977) Reaction of $^3O_2$ with dihydroflavins. 1. N3,5-Dimethyl-1,5- dihydrolumiflavin and 1,5-dihydroisoalloxazines. *J. Am. Chem. Soc. 99*, 7272–7286.
38. Bach, R. D., and Dmitrenko, O. (2003) Electronic Requirements for Oxygen Atom Transfer from Alkyl Hydroperoxides. Model Studies on Multisubstrate Flavin-Containing Monooxygenases. *J. Phys. Chem. B 107*, 12851–12861.
39. Srajer, V., Teng, T., Ursby, T., Pradervand, C., Ren, Z., Adachi, S., Schildkamp, W., Bourgeois, D., Wulff, M., and Moffat, K. (1996) Photolysis of the carbon monoxide complex of myoglobin: Nanosecond time-resolved crystallography. *Science 274*, 1726–1729.
40. Schotte, F., Lim, M., Jackson, T. A., Smirnov, A. V., Soman, J., Olson, J. S., Phillips, G. N., Jr., Wulff, M., and Anfinrud, P. A. (2003) Watching a protein as it functions with 150-ps time-resolved X-ray crystallography. *Science 300*, 1944–1947.
41. Bannwarth, M., Bastian, S., Heckmann-Pohl, D., Giffhorn, F., and Schulz, G. E. (2004) Crystal structure of pyranose 2-oxidase from the white-rot fungus *Peniophora* sp. *Biochemistry 43*, 11683–11690.
42. Hallberg, B. M., Leitner, C., Haltrich, D., and Divne, C. (2004) Crystal structure of the 270 kDa homotetrameric lignin-degrading enzyme pyranose 2-oxidase. *J. Mol. Biol. 341*, 781–796.
43. Kujawa, M., Ebner, H., Leitner, C., Hallberg, B. M., Prongjit, M., Sucharitakul, J., Ludwig, R., Rudsander, U., Peterbauer, C., Chaiyen, P., Haltrich, D., and Divne, C. (2006) Structural basis for substrate binding and regioselective oxidation of monosaccharides at C3 by pyranose 2-oxidase. *J. Biol. Chem. 281*, 35104–35115.
44. Bannwarth, M., Heckmann-Pohl, D., Bastian, S., Giffhorn, F., and Schulz, G. E. (2006) Reaction geometry and thermostable variant of pyranose 2-oxidase from the white-rot fungus *Peniophora* sp. *Biochemistry 45*, 6587–6595.

BI801918U